ELSEVIER

Deep-Sea Research II 53 (2006) 1261–1281

DEEP-SEA RESEARCH
PART II

www.elsevier.com/locate/dsr2

Basin-scale structures governing the position of the deep fluorescence maximum in the Gulf of Cádiz

G. Navarro[a,b,*], J. Ruiz[a], I.E. Huertas[a], C.M. García[b], F. Criado-Aldeanueva[c], F. Echevarría[b,d]

[a]*Departamento de Oceanografía, Instituto de Ciencias Marinas de Andalucía (CSIC), 11510 Puerto Real, Cádiz, Spain*
[b]*Área de Ecología, Facultad de Ciencias del Mar, Universidad de Cádiz, 11510 Puerto Real, Cádiz, Spain*
[c]*Departamento de Física Aplicada II, Universidad de Málaga, Málaga, Spain*
[d]*Centro Andaluz de Ciencia y Tecnología Marinas, 11510 Puerto Real, Cádiz, Spain*

Received 1 March 2006; accepted 7 April 2006

Abstract

Physical and biological properties of the water column in the Gulf of Cádiz area were examined during a survey in May 2001. The sampling region was dominated by the presence of a central warm core and anticyclonic circulation in the open ocean, upwelling processes nearby both Cape Santa María and Cape San Vicente, and a coastal counter current along the continental shelf. These features determined the stratification of the water column and thereby nutrient distribution. A strong positive correlation between a particular isopycnal (with a density of 26.6 kg m^{-3}) and the depth of the Deep Fluorescence Maximum (DFM) throughout the whole basin was found. This isopycnal marked the interface between the deepest limit of the Surface Atlantic Water (SAW) and the shallowest limit of the North Atlantic Central Water (NACW) and was characterized by nutrient concentrations non-limiting for phytoplankton growth. According to this analysis, the isopycnal can be considered as a nutrient tracer in the Gulf, determining the depth at which the DFM is invariably located, with the DFM intensity depending upon advective and diffusive fluxes arising around the interface.

Keywords: Gulf of Cádiz; Physical–biological coupling; Deep fluorescence maximum; Primary production

1. Introduction

The Gulf of Cádiz is a wide basin located southwestern of the Iberian Peninsula connecting the Atlantic Ocean and the Mediterranean Sea through the Strait of Gibraltar. In spite of the particular oceanographic features that take place in the area (García-Lafuente et al., 2006) only a few oceanographic studies had been performed in the area until very recently. Early investigations in the late 60s by Lacombe et al. (1968) and Heezen and Johnson (1969) focused mainly on the distribution of water masses, which were followed by a Meteor cruise in 1971 aimed at quantifying the Mediterranean outflow and its distribution in the Gulf (Zenk, 1975). The first hydrological study carried out in the

*Corresponding author. Departamento de Oceanografía, Instituto de Ciencias Marinas de Andalucía (CSIC), 11510 Puerto Real, Cádiz, Spain. Tel.: +34 956 832612; fax: +34 956 834701.
E-mail address: gabriel.navarro@icman.csic.es (G. Navarro).

0967-0645/$ - see front matter © 2006 Elsevier Ltd. All rights reserved.
doi:10.1016/j.dsr2.2006.04.013

basin to describe the geostrophic flows (Molina, 1975) preceded a study that characterized the oceanographic patterns present in the area through both thermal images and temperatures profiles (Stevenson, 1977). According to these pioneer works and more recent modeling (Johnson and Stevens, 2000), the surface circulation in the Gulf is directly related to the general circulation in the Atlantic Ocean, and particularly, to the Azores current, since one of its branches penetrates in this geographical region.

As pointed out above, the majority of the studies performed in the Gulf have concentrated on the Mediterranean Water outflow through the Strait of Gibraltar (Zenk, 1975; Bryden and Stommel, 1982; Zenk and Army, 1990; Ochoa and Bray, 1991; Baringer and Price, 1999) and its subsequent mixing with Atlantic waters. Moreover, the formation of *eddies* of a Mediterranean origin, the so-called *meddies*, has been also matter of special interest (Bower et al., 1997; Serra and Ambar, 2002; Serra et al., 2002; and references therein).

Biological studies in the basin commenced in the 90s, mainly in the eastern section (Rubín et al., 1997; Prieto et al., 1999; García et al., 2002), with the general objective to correlate hydrological conditions and icthyoplankton dynamics, especially the distribution of the anchovy *Engraulis encrasicolus*. Cruises carried out in summers 1995 and 1997 observed different oceanographic patterns, since during the former a pool of warm water was observed near the mouth of the Guadalquivir River (Rubín et al., 1997; Prieto et al., 1999), whereas in the latter a cold front water was registered in the same area (García et al., 2002). In addition, a persistent upwelling area near Cape Trafalgar was identified, characterized by high concentrations of both nutrient and chlorophyll concentration (Rubín et al., 1999; Prieto et al., 1999; García et al., 2002) and frequent thermal anomalies due to tide–topography interactions (Vargas-Yañez et al., 2002). The distribution of fisheries of local commercial interest, and its connection with the hydrodynamical patterns in the continental shelf bounded between the mouths of Guadiana and Guadalquivir rivers was recently examined (Ruiz et al., 2006; Baldó et al., 2006; Catalán et al., 2006). This sector constitutes an important spawning area for fish species of economical interest and where the meteorological forcing plays a modulating role in primary production (PP) (Navarro and Ruiz, 2006). Furthermore, hydrodynamic conditions also influence both PP and the related air–sea CO_2 fluxes in this particular portion of the continental shelf (Huertas et al., 2005, 2006).

This study was devoted to analyze the relationships between physical and biological variables in order to gain insight into the mechanisms responsible for variations in the productivity of the Gulf. In particular, this investigation concentrates on explaining the formation and position of the deep fluorescence maximum (DFM) in the water column throughout the area between Cape San Vicente and Cape Trafalgar.

2. Materials and methods

2.1. Physical parameters

Samples were taken during the GOLFO-2001 cruise on board R.V. "*Hespérides*". The macroscale leg was carried out from May 17 to 24 and included 58 sampling stations (Fig. 1). At each station, vertical profiles of temperature, salinity and chlorophyll fluorescence were obtained with an Idronaut MK 317 CTD probe, embedded in a rosette used to collect samples at depths of 10, 25, 50, 75, 100 and 200 m. Wind speed and direction, air temperature, solar radiation and atmospheric pressure were obtained at 1-min intervals approximately 10 m above the sea surface with an ANDERAA meteorological station. At daytime, between 8:00 AM and 20:00 PM, photosynthetic available radiation (PAR) profiles were measured with a Satlantic PRR-600 instrument.

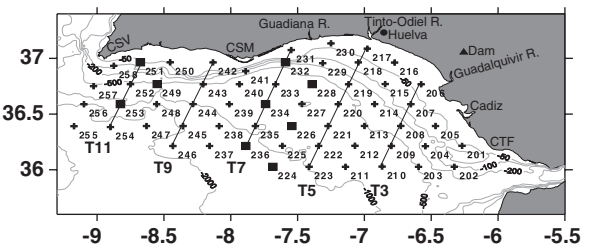

Fig. 1. Map of the study area. Cross symbols indicate the sampling stations and squares locate stations where ^{14}C uptake experiments were performed. Transects are identified by T-numbers. Letters indicate locations and geographic regions referred in the text: CSV—Cape San Vicente; CSM—Cape Santa María; Guadiana River; Tinto-Odiel River, Guadalquivir River; Cádiz Bay; CTF—Cape Trafalgar, Huelva meteorological station (circle symbol) and Alcalá del Río dam (triangle symbol). Bathymetry is indicated by gray lines (25, 50, 100, 200, 500, 1000 and 2000 m).

2.2. Nutrients analysis

Samples for nutrient analysis were filtered through Whatman GF/F, frozen at –20 °C and subsequently analyzed in the laboratory following JGOFS standards (UNESCO, 1994). Nutrients were determined by colorimetric methods using a Technicon autoanalyser TRAACS 800. The depth of the nutriclines for NO_3+NO_2 (Z_{NN}) and PO_4 (Z_{PO_4}) was defined as the shallowest levels at which concentrations were higher than 1 and 0.1 μM, respectively, as previously defined by Morán et al. (2001).

2.3. Chlorophyll

Samples to estimate total chlorophyll *a* (500 ml) were filtered on board through Whatman GF/F (~0.7 μm) filters. To attain the percentage of total chlorophyll corresponding to larger cells (>20 μm), 2–3 l were filtered through a 20 μm mesh net and the fraction collected with a sprayer. The concentrated fraction was then filtered through Whatman GF/F in the same manner as described for total chlorophyll. The pigments retained in the filters were extracted with acetone (24 h, dark, cold storage), and measurements of chlorophyll *a* and phaeopigments were conducted following the methods proposed in the JGOFS protocols (UNESCO, 1994) based on Holm-Hanssen et al. (1965).

2.4. Photosynthesis–irradiance relationships

Photosynthesis–irradiance (*P–E*) experiments were carried out at nine selected stations (Fig. 1). Table 1 indicates the sampling depths. Seawater samples were collected with Niskin bottles at 10 m depth and at the DFM. Fourteen light and one dark (covered with aluminum foil) sterile polystyrene tissue culture bottles (Corning) containing 70-ml water samples were incubated for each experiment in closed linear incubators with circulating water at the in situ sampling temperature (±0.5 °C). Before the incubation, all bottles were spiked with 10 μCi (185 kBq) of $H^{14}CO_3^-$ (NEN, New England Nuclear). Illumination was provided by a slide projector (150 W) and PAR at the position of each incubation bottle was directly measured with a

Table 1
Stations and photosynthetic parameters where *P–E* experiments were performed

St	Z(m)	P_s^B	P_m^B	α^B	β^B	r^2	I_k	K_d	$Z_{1\%}$
224	10	1.3203	1.3203	0.0213	0	0.77	62	0.0534	86
	100	0.4973	0.4518	0.0379	0.0010	0.89	13	0.0534	86
226	10	4.9859	4.9859	0.0182	0	0.99	273	0.0718	64
	50	3.3027	3.2244	0.0904	0.0004	0.92	37	0.0718	64
228	10	1.4136	1.4136	0.0359	0	0.95	39	0.0590	78
	60	0.5224	0.4987	0.1287	0.0130	0.88	4	0.0590	78
232	10	3.0290	3.0290	0.0269	0	0.98	112	0.1132	41
	25	2.5959	2.3585	0.0379	0.0010	0.98	68	0.1132	41
234	10	5.9355	5.9355	0.0615	0	0.98	97	0.0644	71
	60	2.6691	2.3209	0.0665	0.0030	0.97	40	0.0644	71
236	10	4.1604	4.1604	0.0238	0	0.97	174	0.0485	95
	100	0.9461	0.7061	0.0314	0.0050	0.94	30	0.0485	95
249	10	4.7097	4.7097	0.0422	0	0.97	112	0.0636	72
	50	1.885	1.6856	0.0612	0.0020	0.96	31	0.0636	72
251	10	3.1160	3.1160	0.0235	0	0.97	133	0.1316	35
	25	1.958	1.9022	0.0359	0.0002	0.99	54	0.1316	35
253	10	2.0690	2.0690	0.0227	0	0.98	91	0.1086	42
	25	0.1915	0.1714	0.0031	0.0001	0.98	62	0.1086	42

St: station; Z(m): depth were ^{14}C uptake experiment were performed. *P–E* parameters: $P^B_{m,S}$(mg C mg Chl^{-1} h^{-1}); α^B, β^B [mg C mg Chl^{-1} h^{-1}(μmol quanta m^{-2} s^{-1})$^{-1}$]; r^2 is the coefficient of determination; I_k (μmol quanta m^{-2} s^{-1}); K_d (m^{-1}) is attenuation coefficient and $Z_{1\%}$ (m) is the depth of the photic depth.

Hansatech Quantitherm light meter placed inside each bottle. PAR values ranged from 5 to 1500 μmol quanta $m^{-2} s^{-1}$. The desired attenuation of the irradiance received by the bottles was achieved by using several neutral density filters. After 2–3 h incubation, water was filtered through Whatman GF/F filters glass fiber (25 mm) under vacuum pressures <100 mmHg. The measurement of labeled organic carbon retained on glass fiber filters provides an estimation of the total PP rather than the particulate fraction, because of adsorption of photosynthate released as dissolved organic carbon (Morán et al., 1999). Filters were exposed to fuming HCl (35%) for ca. 12 h and left to dry prior to placing into vials. Subsequently, 4.5 ml of *Packard Ultima Gold* liquid scintillation cocktail was added to the vials. Radioactivity was determined in a Wallac 1414 liquid scintillation counter on board and disintegrations min^{-1} calculated with the external standard method. Before further calculations, black-bottle values were subtracted from the light-bottle values for correction of non-photosynthetic ^{14}C fixation. Since photoinhibition was absent in surface samples but present in the majority of deeper samples, different versions of the model that describes the *P–E* relationship were used. Fitting was made by non-linear least-squares regression. Surface data were fitted by the model of Webb et al. (1974):

$$P^B = P^B_m \left[1 - \exp\left(-\frac{\alpha^B I}{P^B_m}\right)\right], \quad (1)$$

where P^B(mg C mg $Chl^{-1} h^{-1}$) is the chlorophyll *a*-normalized photosynthetic rate, P^B_m (mg C mg $Chl^{-1} h^{-1}$) corresponds to the maximum chlorophyll *a*-normalized photosynthetic rate and α^B[mg C mg $Chl^{-1} h^{-1}$ (μmol quanta $m^{-2} s^{-1})^{-1}$] represents the chlorophyll *a*-normalized initial slope of the *P–E* curve.

DFM data were fitted by the model of Platt et al. (1980):

$$P^B = P^B_s \left[1 - \exp\left(-\frac{\alpha^B I}{P^B_s}\right)\right] \left[\exp\left(-\frac{\beta^B I}{P^B_s}\right)\right], \quad (2)$$

where P^B_s (mg C mg $Chl^{-1} h^{-1}$) is the maximum chlorophyll *a*-normalized photosynthetic rate without photoinhibition and β^B (same units as α^B) represents the photoinhibition parameter. The rest of parameters are like those described in the previous model. If β^B becomes 0 (i.e., no photoinhibition), P^B_s in the Platt et al. (1980) model would then be equivalent to P^B_m in the model proposed by Webb et al. (1974). The relationship between the photosynthetic parameters P^B_m, α^B and β^B, physical variables and nutrient concentration was explored by a correlation matrix.

2.5. Integrated PP

The *P–E* parameters, together with PAR and chlorophyll *a* depth profiles, and the daily irradiance were used to estimate the daily rates of depth-integrated PP (PP_{int}); integration down to 100 m depth was performed by the trapezoidal method following Platt et al. (1990). A linear regression between the surface and deep *P–E* values at each station was used to obtain an estimate of their variation through the corresponding depth range (Morán et al., 2001; Morán and Estrada, 2001). The *P–E* values measured at the DFM were maintained constant for the rest of the water column below.

3. Results

3.1. Water masses and circulation framework

The general surface circulation during the sampling period, displayed in Fig. 2, was predominantly anticyclonic with some mesoscale meanders. At about 7.5°W (off Cape Santa María), the main current bifurcated into two branches: one turned to the southeast and subsequently to the northeast and the other continued flowing parallel to the Spanish coast. The two branches joined downstream at about 7°W and followed two paths when approaching the Strait of Gibraltar: one entered the Mediterranean Sea through the Strait to balance evaporation and buoyancy losses within the Sea and the other formed an anticyclonic meander in the easternmost region, which finally met the Canary Current further southeast (out of the scope of the survey).

The ocean surface at the central region of the basin was occupied by a core of warm and saltier Surface Atlantic Water (SAW), where velocities were generally slow (Criado-Aldeanueva et al., 2006). In addition, upwelling areas were found at Cape San Vicente and Cape Santa María, which were identified by waters of lower temperature and salinity (Criado-Aldeanueva et al., 2006). In Cape San Vicente a large cyclonic eddy was detected, associated with the upwelling event (García-Lafuente et al., 2006). On the eastern part of the shelf,

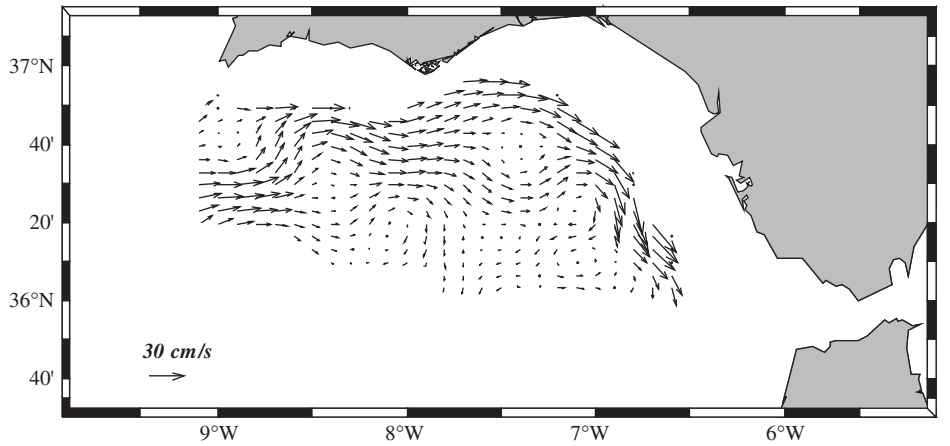

Fig. 2. Geostrophic velocity at 10 m depth referred to 300 m from Macroscale data. The circulation pattern is described in the text.

the coastal counter current was observed (García-Lafuente et al., 2006). The temperature and salinity fields exhibited some mesoscale meanders until about 150 m depth. The most outstanding, the filament of Cape Santa María, stretched southwards off the cape and was attributable to the advection of upwelled North Atlantic Central Water (NACW) from the Cape San Vicente upwelling area (Criado-Aldeanueva et al., 2006). During the cruise, a seasonal thermocline was present, mainly observed in the open sea region.

Criado-Aldeanueva et al. (2006) show that the surface temperature, and hence density, fields were rather wind-dependent. Some hydrological features, such as the upwelling off Cape Santa María or the surface signature of the Huelva Front, were enhanced under westerlies, but they weakened or even disappeared under easterlies. In contrast, easterlies favoured the development of a coastal counter current that advected warm waters westwards and flooded the easternmost basin on the surface, thus confining the upwelled water to a smaller region west of Cape Santa María. The wind variations only affected a relatively shallow layer (<50 m). Below this surface layer, the hydrological characteristics were fairly independent of meteorological forcing. Additionally, the variations of geostrophic transports (referred to 300 m) were also correlated with wind: under westerlies the volume transport in any north–south section was about 30% greater than under easterlies (Criado-Aldeanueva et al., 2006).

Different water masses were found in the Gulf of Cádiz (Criado-Aldeanueva et al., 2006): (i) NACW that presented a linear behavior in the T–S diagram, with temperature ranging between 11 and 17 °C and salinity varying from 35.6 to 36.5. Below a certain depth, the T–S diagram diverged from this linear behavior because of the presence of waters with; (ii) Mediterranean origin (MW) that have a very high salinity. On the surface and shallow depths were the (iii) SAW, considered by some authors as a modification of NACW due to stratification and air–sea interactions. SAW can be characterized for practical purposes as a region in the T–S diagram with temperatures above 16 °C and $S \approx 36.4$, and it was found between the surface and a depth of approximately 100 m. At some of the sampled stations, warm surface waters (SW), possibly influenced by the continental shelf and, to a lesser extent by fluvial factors, were detected. They corresponded to the points of the T–S diagram with temperatures $14\,^{\circ}\mathrm{C} \leqslant T \leqslant 18\,^{\circ}\mathrm{C}$ and salinities $35.9 \leqslant S \leqslant 36.5$ that fell outside the straight line of NACW.

3.2. Physico-chemical and biological variables distribution

3.2.1. PAR distribution

The photic depth ($Z_{1\%}$), defined as the depth at which the radiation is 1% of the surface incident radiation, is shown displayed in Fig. 3. Overall, the photic layer was observed to increase gradually from the coast towards oceanic stations, deepening towards the offshore stations. The mean value for the photic depth in the whole area was 60 m, but only 20–25 m at coastal stations located between

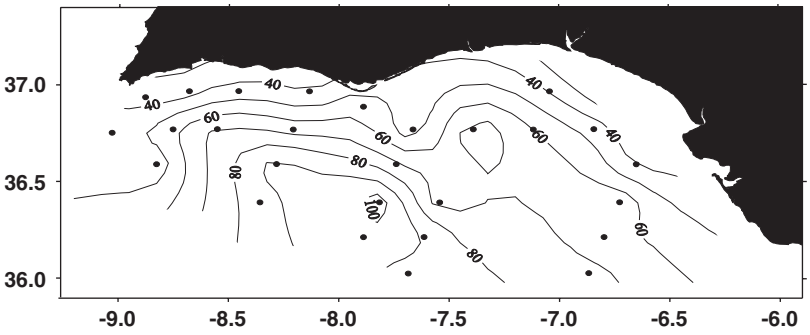

Fig. 3. Contour map of the photic depth ($Z_{1\%}$) expressed in meters at stations where PAR profile was measured (black circles).

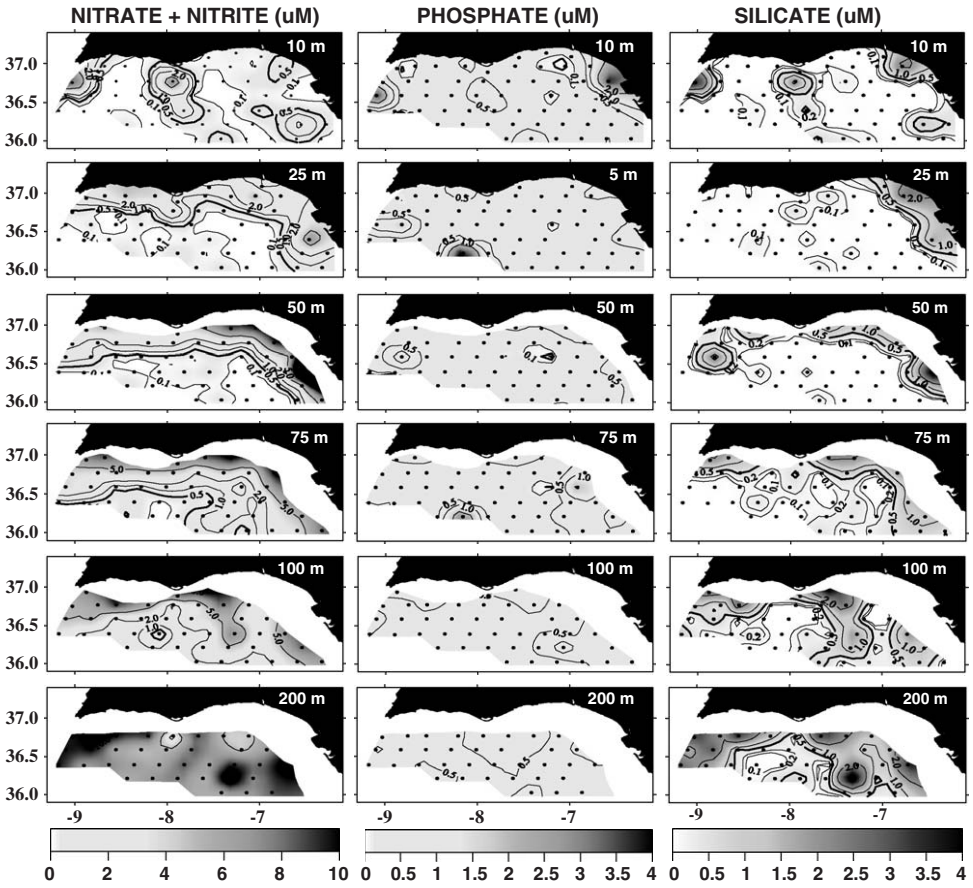

Fig. 4. Distribution of nitrate plus nitrite (μM), phosphate (μM) and silicate (μM) at 10, 25, 50, 75, 100 and 200 m depths in the Gulf of Cádiz during the Macroscale leg in GOLFO-2001 Cruise.

Cádiz and Huelva (around 20–25 m), coinciding with the maximum chlorophyll concentrations. Near Cape San Vicente the photic layer was of around 35 m, and a maximum depth was reached in oceanic stations, with values of 75 m or even approaching 100 m in certain areas.

3.2.2. Nutrient distribution

The highest nitrate and nitrite concentrations at 10 m depth (~1.5 μM) were found in stations around Capes San Vicente, Santa María and Trafalgar (Fig. 4). These levels are similar to the value of the semisaturation constant given for

diatoms (Ks = 1–1.5 μM; Walsh, 1988) and clearly higher than the general value of 0.5 μM proposed by Eppley et al. (1969). Lower concentrations were detected in the rest of the basin at that particular depth. In contrast, the nutrient distribution at 25 m depth clearly changed (Fig. 4), with the highest concentrations being measured in coastal stations (>2.0 μM) and lower concentrations in oceanic sites. As depth increased, the surface area containing concentrations >0.5 μM also increased, and at 100 m no limiting concentrations for phytoplankton growth were found in the sampling region (Fig. 4).

With respect to phosphate, maximum concentrations were located at 10 m depth near the mouth of the Tinto-Odiel River and the Bay of Cádiz, as well as in stations close to Cape San Vicente. These maxima are possibly related to anthropogenic inputs, as phosphates usually enter into marine environments by river discharge. The measured values exceeded the semisaturation constants for phytoplankton growth (Ks) of 0.03 and 0.05 μM reported by McAllister et al. (1964) and Davies and Sleep (1981), respectively. Similarly, phosphate concentrations were always higher than the Ks values in the rest of the water column throughout the entire sampling area and similar to other values detected previously in San Vicente and Santa María areas (Cotté-Krief et al., 2000).

Silicate distribution is also depicted in Fig. 4. At 25 m, maxima were observed in the coastal area between Cádiz and Huelva, probably due to inputs from river discharge. As a general trend, concentrations increased with depth and minimum levels were found in oceanic stations. In the majority of the basin, the silicate concentration was lower than the semisaturation constant for phytoplankton growth (Ks = 2.0 μM) proposed by Brzezinski et al. (1998), although these levels were higher to the value considered limiting for diatom growth (0.5 μM, Paasche, 1973; 0.96 μM, Brzezinski et al., 1998).

The nutricline depth of nitrate plus nitrite (Z_{NN}, see Section 2.2) showed a gradual increase from inshore to offshore stations (Fig. 5A). In the coastal area, Z_{NN} was at about 20–30 m, whereas in the open-ocean region it deepened to approximately 100 m. The average nutricline depth for the entire basin was calculated to be 54 m.

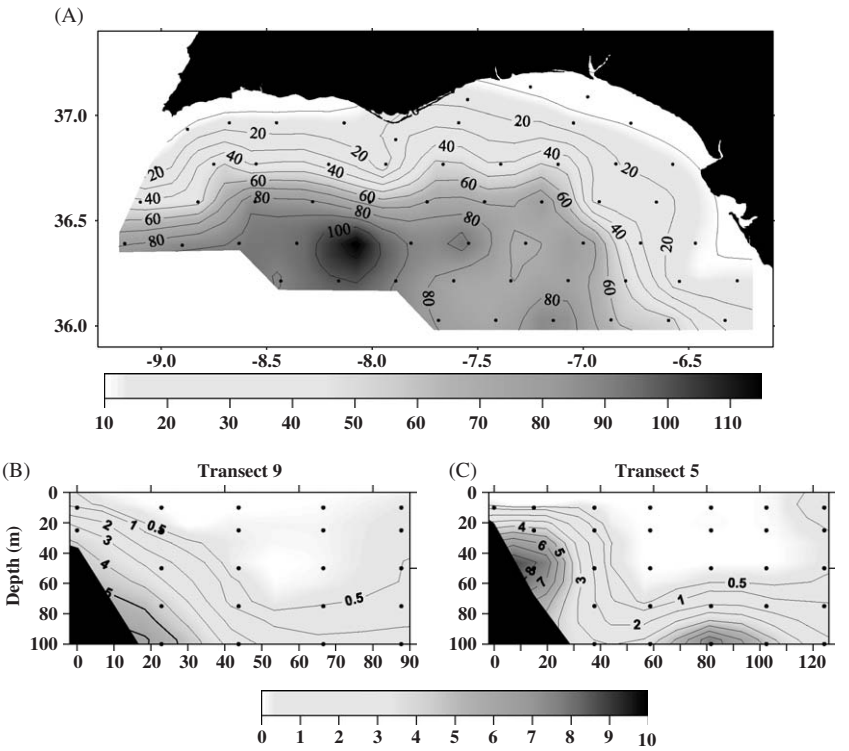

Fig. 5. (A) Spatial distribution of Z_{NN} expressed in meters. Vertical distribution of nitrate plus nitrite (μM) for Transect 9 (B) and Transect 5 (C) are also shown. X-axis indicates distance (Km) from the coastal station.

Different transects were selected to display the vertical distribution of nitrate plus nitrite. Nutrient concentration isopleths were observed to upraise towards the coast, similar to the pattern exhibited by the isopycnals (García-Lafuente et al., 2006). Several mechanisms could be proposed to explain the isopleths distributions, such as the occurrence of upwelling processes on the west around Cape San Vicente, mesoscale activity in the center of the basin or remineralization mechanisms on the east side, and also terrestrial inputs. Moreover, the observed trend in the coastal sector could be attributed to the upwelling of nutrient-rich cold waters. In fact, a strong negative correlation between temperature and nutrient concentration was found, which was statistically significant ($r = -0.78$, $p < 0.001$ y $n = 281$).

3.2.3. *Chlorophyll distribution*

The distribution of chlorophyll fluorescence and total chlorophyll presented parallel patterns (Fig. 6). Maximum values of both variables were detected near Cape Trafalgar at 10 m depth ($>2.5\,\mathrm{mg\,Chl\,m^{-3}}$ for total chlorophyll and 0.4 r.u. for fluorescence). Furthermore, the coastal area in the vicinity of Cape Santa María showed high chlorophyll and fluorescence levels at 25 m. These chlorophyll maxima coincided with maxima in nutrient distribution, mainly nitrate plus nitrite (Fig. 4). In the center of the basin, where an anticyclonic circulation usually occurs, minima of both fluorescence and chlorophyll were measured since nutrient concentrations were limiting for phytoplankton growth. The distribution of both

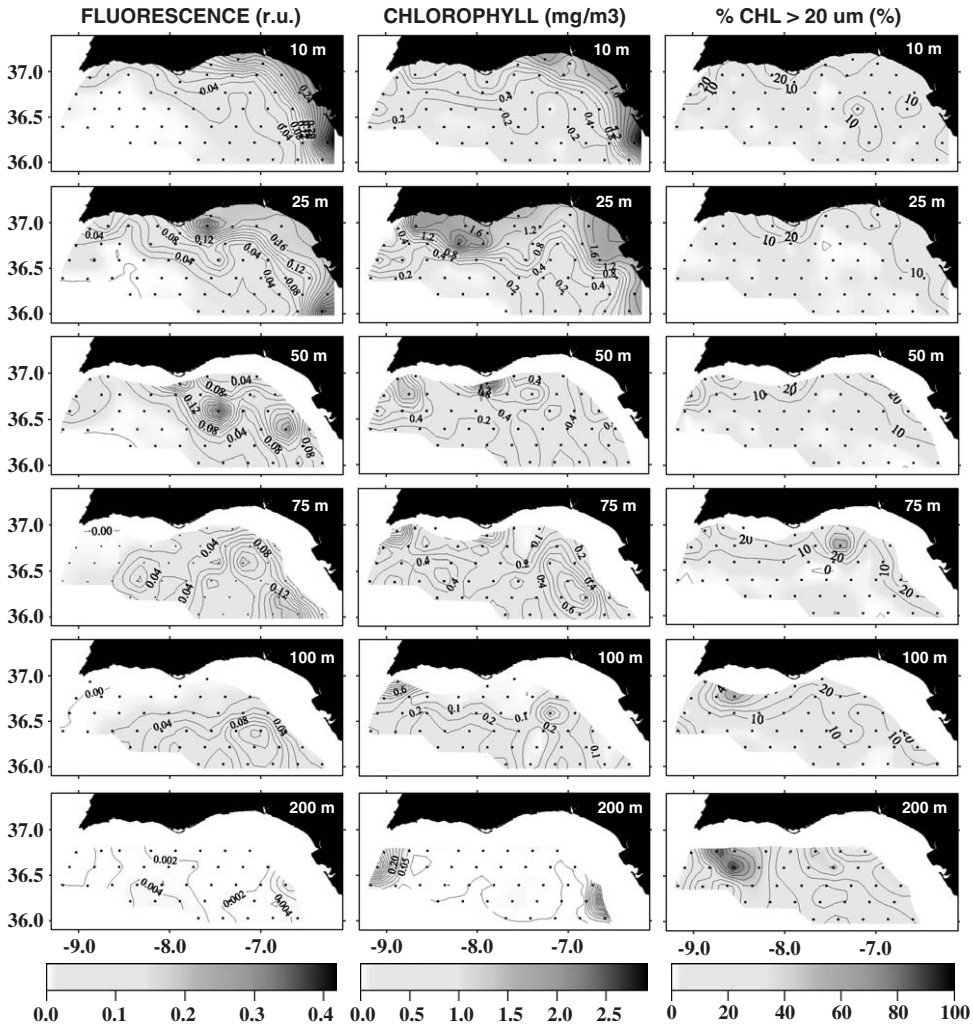

Fig. 6. Distribution of fluorescence (relative unit, r.u.), chlorophyll *a* ($\mathrm{mg\,Chl\,m^{-3}}$) and percentage of total chlorophyll contained in cells >20 μm (%) at 10, 25, 50, 75, 100 and 200 m depths in the Gulf of Cádiz during the Macroscale leg in GOLFO-2001 Cruise.

variables exhibited mesoscale meanders, similar to those found for temperature and salinity (Criado-Aldeanueva et al., 2006) and as depth increased, total chlorophyll and fluorescence decreased. Fig. 6 also depicts the percentage of large cells, corresponding to a fraction of total chlorophyll. Maxima were observed in stations close to Capes Trafalgar and Santa María.

The depth of the DFM (Z_{DFM}) has been plotted in Fig. 7A Z_{DFM} was found to be very similar to Z_{NN} (Fig. 5A), and the greatest depths of the former ($\approx$90 m) appeared in open sea stations, diminishing inshore (around 20–30 m).

3.2.4. Primary production

Photosynthetic parameters at the nine stations where *P–E* experiments were carried out are shown in Table 1, and *P–E* curves have been plotted in Fig. 7. All the parameters showed significant differences between surface waters and the DFM depth: *t*-test ($n = 9$) P^B ($p = 0.0056$), α^B ($p = 0.0435$) and I_k ($p = 0.0015$) (Fig. 8). At each station, maximum photosynthetic rates (P^B_m) were always higher in surface waters (average 3.3846 mg C mg Chl^{-1} h^{-1}) than at the DFM (average 1.6187 mg C mg Chl^{-1} h^{-1}). Maximum values for P^B_m at surface were found at stations 234, 226 and 249 ($>$4.5 mg C mg Chl^{-1} h^{-1}), whereas maximum values at the DFM were measured at stations 226, 232 and 234 ($>$2.5 mg C mg Chl^{-1} h^{-1}). These values are in the same order of magnitude as those reported in a coastal fringe of this area (Huertas et al., 2005). The maximum light utilization coefficient or initial slope of the *P–E* curve (α^B) was 1.7-fold higher at the DFM than at the surface (averages 0.0546 [mg C mg Chl^{-1} h^{-1}(μmol quanta m^{-2} s^{-1})$^{-1}$] and 0.0307 [mg C mg Chl^{-1} h^{-1}(μmol quanta m^{-2} s^{-1})$^{-1}$]) respectively, Fig. 9). At station 253, located near Cape San Vicente, surface α^B was higher than α^B at DFM depth.

As expected, the light-saturation parameter, I_k, was always higher at the surface (average 121 μmol quanta m^{-2} s^{-1}) than at the DFM (average 38 μmol quanta m^{-2} s^{-1}). The minimum value was found at station 228 at 60 m depth (4 μmol quanta m^{-2} s^{-1}). Photoinhibition (β^B) was observed

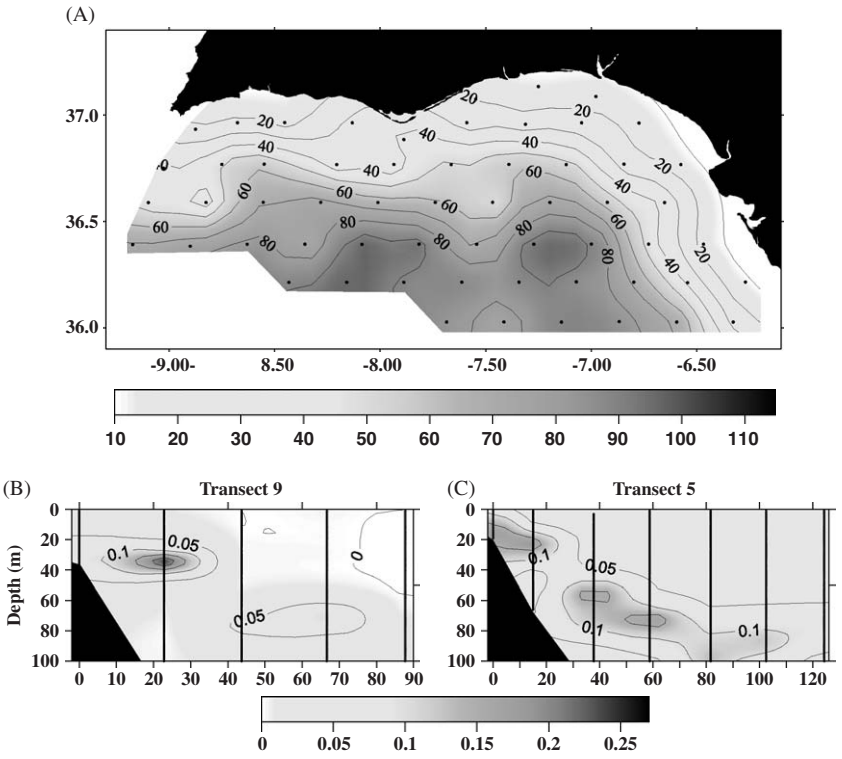

Fig. 7. (A) Spatial distribution of the Z_{DFM} expressed in meters. Vertical distribution of fluorescence (r.u.) for Transect 9 (B) and Transect 5 (C) are also given. X-axis indicates distance (Km) from the coastal station.

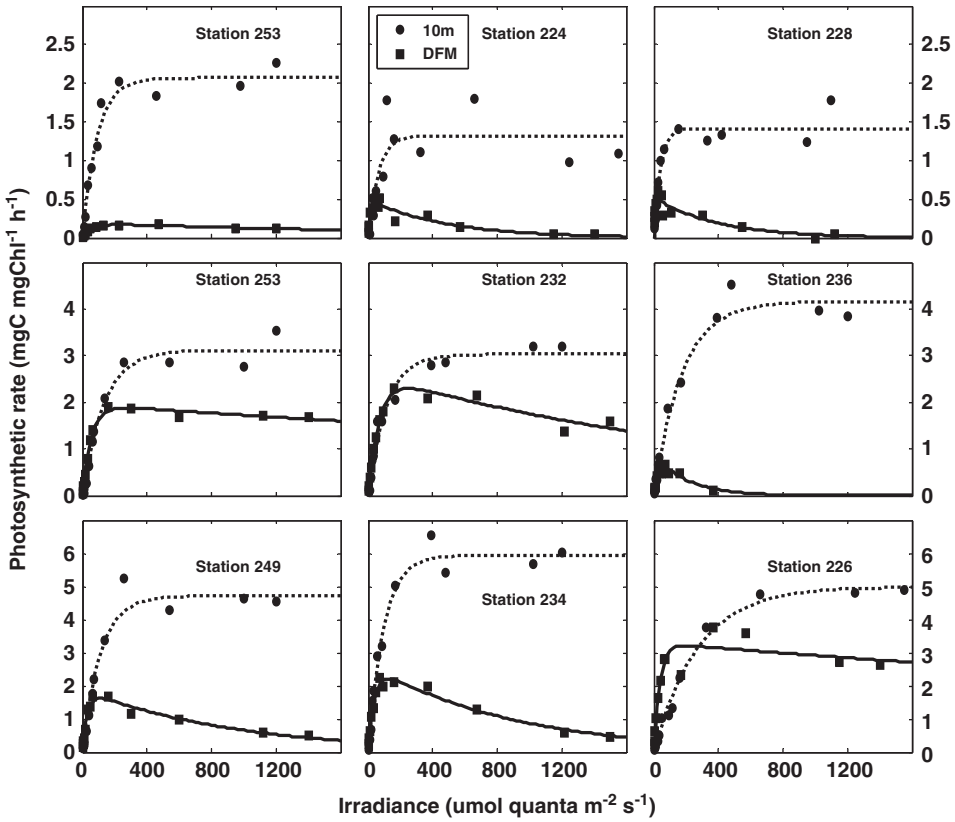

Fig. 8. Photosynthesis–irradiance relationships at 10 m (circles and dotted line) and the depth of DFM (squares and solid line) in nine stations where primary production was measured.

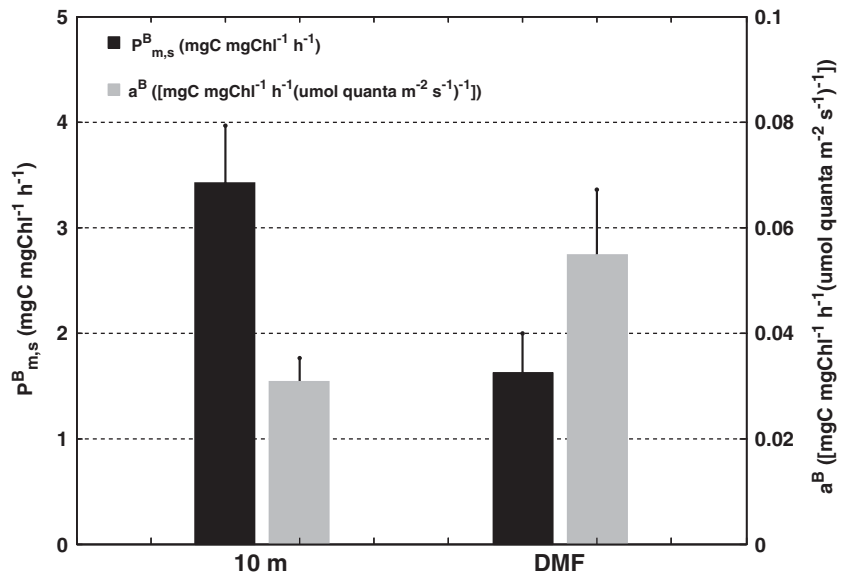

Fig. 9. Average and standard error for $P^{B}_{m,s}$ (black bars) and α^{B} (grey bars) at 10 m depth (left) and DFM (right) at the stations where primary production experiments were conducted.

Table 2
Matrix of correlations between *P–E* parameters and diverse physico-chemical variables[a]

	Depth	Temp.	Salinity	Density	NN	PO_4
P^B_m	−0.5445*	0.2860	−0.1984	−0.5164*	−0.5052*	−0.1571
α^B	0.3795	−0.3235	0.0345	0.4458	0.5430*	−0.3119
β^B	0.3100	0.1389	0.2950	0.2074	0.6118	−0.2876
I_k	−0.6051**	0.4300	−0.1382	−0.6647**	−0.5096*	0.0218

*$p<0.05$.
**$p<0.01$.
[a]Depth, temperature, salinity, density, NN, PO_4: in situ values. $n=18$ for P^B_m, α^B, I_k. $n=9$ for β.

Table 3
Primary production rates for station where *P–E* relations was calculated

St	P. production ($mg\,C\,m^{-2}\,d^{-1}$)
224	150.42
226	617.54
228	531.00
232	510.44
234	757.83
236	272.18
249	603.62
251	895.25
253	163.20

in all the DFM samples, although at station 253, β^B was very low ($0.0001\,mg\,C\,mg\,Chl^{-1}\,h^{-1}$ [$\mu mol\,quanta\,m^{-2}\,s^{-1}$]$^{-1}$). Station 228 exhibited the highest value of photoinhibition ($0.0130\,mg\,C\,mg\,Chl^{-1}\,h^{-1}$[$\mu mol\,quanta\,m^{-2}\,s^{-1}$]$^{-1}$), and the rest of the values were found to be one order of magnitude lower. This pattern can be explained based on the adaptation of phytoplankton to low light environments, as cells have the capacity to adapt to different light regimes under conditions of stratification in the water column. In fact, strong correlations were found between P^B_m and I_k with variables that fluctuate with depth as temperature, density, nitrate and nitrite concentrations (Table 2).

3.2.5. Integrated PP

Table 3 summarizes the integrated PP (PP_{int}) values. The values ranged between 150 and $895\,mg\,C\,m^{-2}\,d^{-1}$, with an average value of $500\,mg\,C\,m^{-2}\,d^{-1}$. Highest values were observed at stations 226, 234, 249 and 251 ($>600\,mg\,C\,m^{-2}d^{-1}$), whereas the lowest PP_{int} were measured at oceanic stations such as 224, 236 and 253 ($<300\,mg\,C\,m^{-2}\,d^{-1}$). These values are in agreement with those measured in other subtropical domains in the Atlantic Ocean during AMT cruises between 30°N and 40°N and corresponding to 125–500 $mg\,C\,m^{-2}\,d^{-1}$(Marañón et al., 2000). In the Gulf of Cádiz, higher values were found in upwelling areas, around the Capes San Vicente and Santa María. The rates observed were higher than others normally attained in oligotrophic domains and the same order of magnitude as the levels reached in upwelling areas such as the Saharan upwelling where Basterretxea and Arístegui (2000) reported PP_{int} rates of 102 and $5326\,mg\,C\,m^{-2}\,d^{-1}$. Also, in the Galician upwelling during summer Joint et al. (2002) found rates of $1300\,mg\,C\,m^{-2}\,d^{-1}$ in the coastal area, $700\,mg\,C\,m^{-2}\,d^{-1}$ on the continental slope, and $290\,mg\,C\,m^{-2}\,d^{-1}$ in oceanic waters. In addition, PP_{int} values of $800\,mg\,C\,m^{-2}\,d^{-1}$ have been estimated in a shallow area of the Gulf of Artrabo (NW Spain) (Bode and Varela, 1998). Therefore, the PP_{int} rates observed in the sampled region in the Gulf Cádiz reflect the sub-tropical location of the basin, with a few sites displaying higher rates because of the presence of sub-regional dynamics.

The low observed PP rates offshore sites reflected the reduced chlorophyll concentrations present in the water column. Moreover, in that area, the DFM was located at depths where the light intensity was also very reduced (Fig. 3). As an example, the station 224 (Fig. 10) showed that the Z_{NN} was situated at 80 m depth, coinciding with the DFM. At that level, PP was very low, as only 1% of the incident irradiance reached that particular depth. In contrast, at inshore stations (e.g., 251, Fig. 10), where isopycnal upwelling allows a nutrient input into surface layers ($Z_{NN}=15\,m$), DFM was at a shallower depth. This led to a rise in PP_{int} since the incident radiation was higher than I_k and also phytoplankton population proliferated. The only

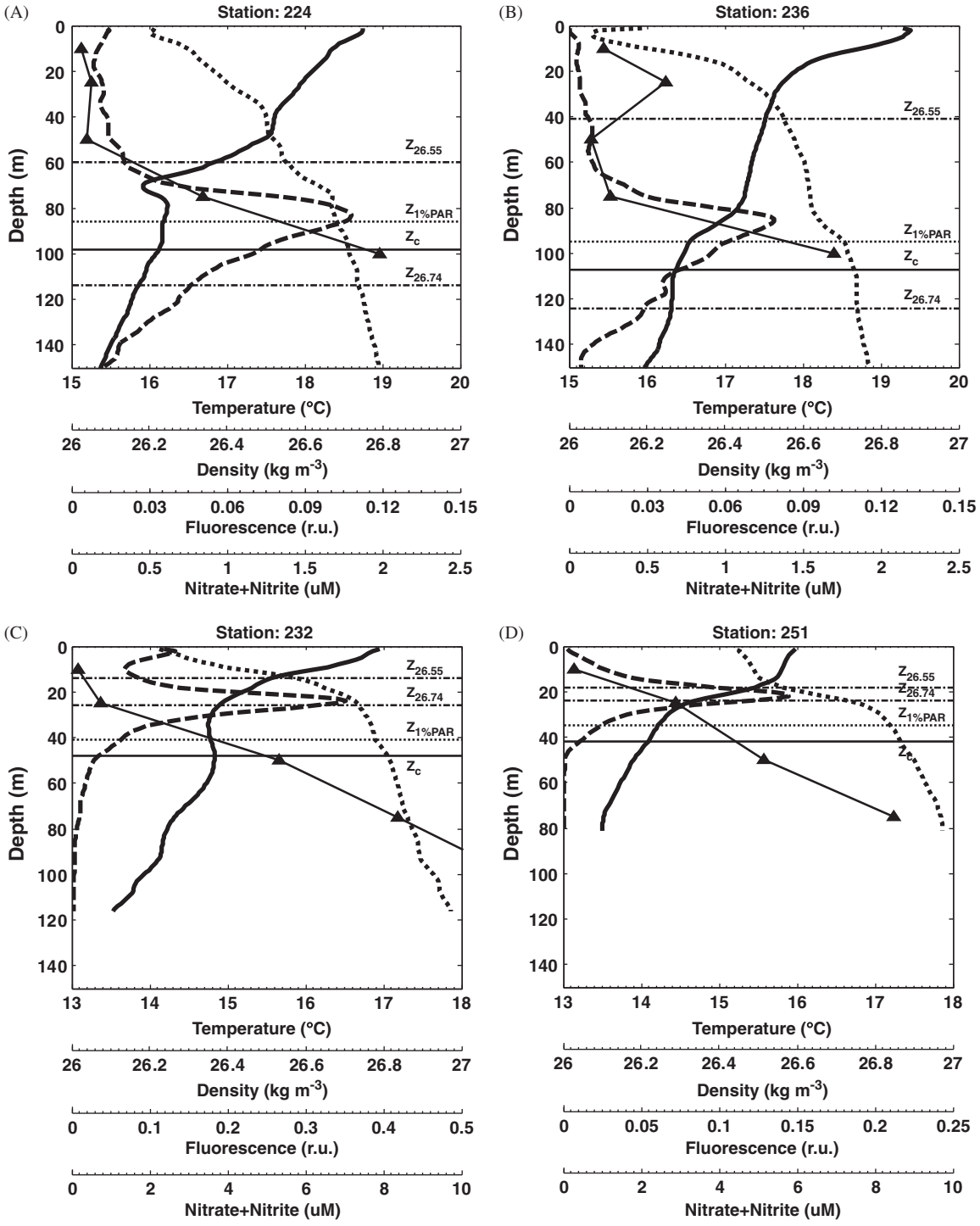

Fig. 10. CTD profiles (temperature, solid line; fluorescence, dashed line and density, dotted line) at four stations of the sampling grid. Nitrate + nitrite concentration is represented by triangles and solid line. Horizontal lines show the compensation depth (Z_c), 1% surface PAR ($Z_{1\%\ PAR}$) and the depths of the σ_t values of 26.55 ($Z_{26.55}$) and 26.74 ($Z_{26.74}$).

significant correlation found between PP_{int} and physical and biological variables corresponded to surface temperature, which would indicate the increase of PP_{int} in upwelling areas.

4. Discussion

Data presented in this work show that the distribution of the biological variables considered was fundamentally forced by the hydrodynamic regime present in the basin during the sampling period. In the open sea, surface waters had characteristics of SAW and the DFM was located around 85 m, coinciding with the depth of the nutricline and lying several meters above the photic layer. In the upper layer, phytoplankton activity exhausted nutrient after winter deep mixing (Navarro and Ruiz, 2006). This limitation was reflected in the low values of fluorescence observed above 65 m, which increased gradually downward until reaching the DFM at 85 m, coinciding with the limit of the photic layer (Fig. 10A,B). Therefore, in the water column two well-differentiated layers could be distinguished: an upper one characterized by low nutrient concentrations and enough light intensity to support phytoplankton growth, and a lower nutrient-rich deeper layer where light was limiting for phytoplankton proliferation. The apparition of a permanent DFM is a typical structure in the North Atlantic gyre (e.g., Fasham et al., 1985; Agustí and Duarte, 1999). The total chlorophyll values found in this area over the upper 50 m (Fig. 6) were similar to those measured normally in oligotrophic waters (chlorophyll $< 0.2\,mg\,m^{-3}$) (Herbland and Le Boutellier, 1981; Furuya, 1990; Agustí and Duarte, 1999) and PP rates were also equivalent to others reported previously in oligotrophic environments ($\approx 100\,mg\,C\,m^{-2}\,d^{-1}$; Mann and Lazier, 1996).

In the northern sector and situated in the proximities of Cape San Vicente, an upwelling occurred (Criado-Aldeanueva et al., 2006) that led to the shoaling of the isopycnals, thereby enhancing the input of nutrients to surface waters (Figs. 4 and 5) and the PP rates (Table 3). The upwelling is generally detected as a permanent structure during the summer period, induced by the persistence of northerly winds in the area during this season (Wooster et al., 1976; Fiúza et al., 1982; Folkard et al., 1997). The presence of filaments with distinctive temperature (Relvas and Barton, 2002) and chlorophyll (Peliz et al., 2004) patterns has been detected in the past off Cape San Vicente. In this study, the filaments appeared at the end of the sampling period, being even detected by remote sensing (not shown).

The general pattern in the basin can be then summarized by the presence of a wide warm core in the center of an anticyclonic meander (Criado-Aldeanueva et al., 2006). This structure is perturbed in the northern part of the Gulf, close to the coast, by diverse processes. The biological response to the physical structures is evident not only by the observed increase in surface chlorophyll and PP in areas submitted to coastal influence, but also by the vertical pattern of these variables. In particular, the depth of the DFM was observed to decrease in response to the general isopycnal shoaling observed in the center and that propagates towards the north (Figs. 6 and 7). Despite the wide depth range displayed by the DFM position (19–98 m depths, Fig. 11A), this one occurred mostly in a narrow density range (Fig. 11B). Fig. 11A illustrates the high positive correlation found between the DFM and a particular density range, regardless of the depth at which the DFM appears. Defining the upper and lower limits of the DFM as the least and greatest depths at which fluorescence was 50% or more than the maximum in a given profile (Tett et al., 2002), the observed maxima fell within a σ_t range of 26.55 ± 0.02 and 26.74 ± 0.02, respectively, with the average σ_t value being 26.66 ± 0.01. Strong positive correlations also were found between the depth of that particular isopycnal and some singular depths relevant for biological variables (Table 4).

Several mechanisms might be claimed as factors in determining the presence of the DFM at a certain isopycnal rather than at a certain depth. It could be argued that at this density an abrupt change of density in the water column takes place. It has been proposed that in zones characterized by a steep density gradient, fluorescence increases as a result of phytoplankton accumulation and the subsequent cell photoadaptation (e.g., Cullen, 1982). Fig. 12 demonstrates no clear relation between the intensity of the pycnocline, estimated by Brunt–Väisälä frequency, and σ_t values around 26.66. Therefore, it seems unlikely that the increase in fluorescence on that isopycnal could be due to changes in the stability of the water column.

On the other hand, light limitation for phytoplankton growth in both open-ocean and coastal areas could explain the location of the DFM. Fig. 10 shows the profile of several variables at

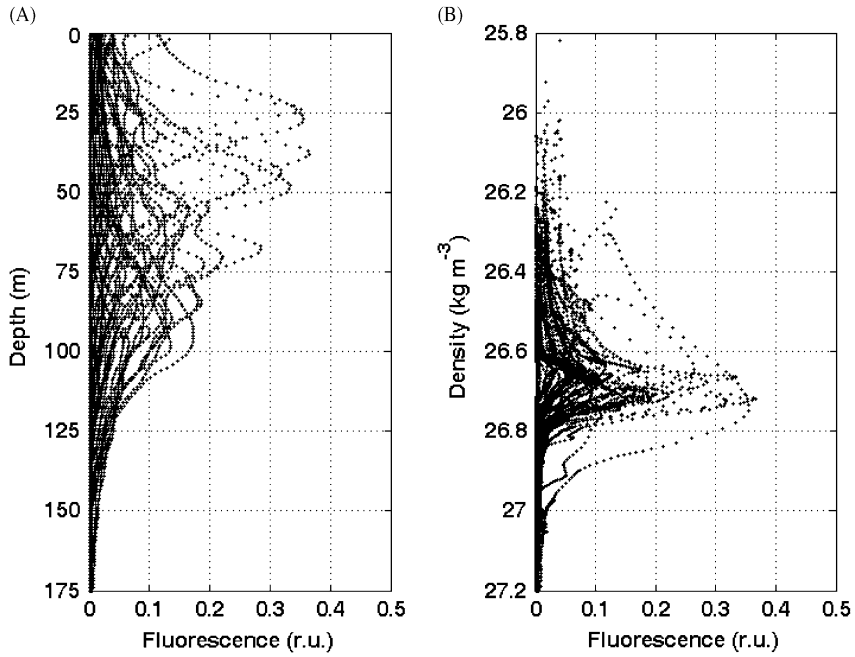

Fig. 11. Depth versus fluorescence (A) and density versus fluorescence (B) profiles at stations with bathymetry higher than 100 m in the Macroscale legs during GOLFO-2001 cruise.

Table 4
Matrix of correlations between some different depth[a] (m)

	Z_{DFM}	Z_{MLD}	$Z_{1\%}$	$Z\,\sigma_{t26.66}$	Z_{NN}	Z_{PO_4}
Z_{DFM}	—					
Z_{MLD}	0.0921	—				
$Z_{1\%}$	0.8984**	0.0319	—			
$Z\sigma_{t26.66}$	0.9314**	0.3116*	0.8464**	—		
Z_{NN}	0.8809**	0.2063	0.7898**	0.8890**	—	
Z_{PO_4}	0.0212	−0.0149	−0.1239	−0.0222	0.0482	—

*$p<0.05$.
**$p<0.001$.
[a]Abbreviations explained in the text.

different stations analyzed in relation to some light-related parameters. The compensation irradiance (I_c) was calculated with the equation:

$$I_c = \frac{r_{0a}}{\chi \alpha_m}, \quad (3)$$

where r_{0a} is the basal respiration rate of phytoplankton ($0.05\,d^{-1}$; Tett et al., 2002), α_m is the maximum photosynthetic efficiency computed using the P–E parameters and χ is the phytoplankton chlorophyll:carbon ratio ($0.4\,mg\,Chl\,mmol\,C^{-1}$, Tett et al., 2002). Compensation depth was also obtained from Lambert–Beer equation (Kirk, 1994):

$$Z_c = \frac{-\ln(I_o/I_c)}{K_d}, \quad (4)$$

where K_d is the attenuation coefficient at each station (Table 1), I_o is the surface radiation and I_c is the compensation irradiance calculated as indicated.

Previous studies have suggested that the occurrence of the DFM above the nutricline is determined by the irradiance, since phytoplankton cells would proliferate in depths close to I_c, where nutrients become available (Riley et al., 1949). In

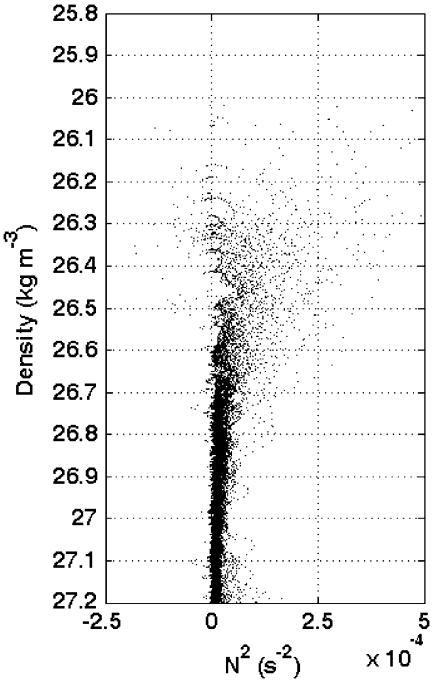

Fig. 12. Density versus N^2 (Brunt-Väisälä frequancy) profiles at all stations of the sampling grid of the Macroscale legs.

open, unperturbed ocean stations in the Gulf, both the compensation depth and the DFM were invariably located between the isopycnals 26.55 and 26.74 ($\sigma_{t26.55-26.74}$). Consequently, light limitation could explain the presence of the DFM at this particular density range simply by the fact that Z_c fell within that interval. However, when the analysis was undertaken for perturbed stations influenced by coastal processes, the DFM remained within the same isopycnal interval, even though its depth was shallower than in open-unperturbed stations (Fig. 10) and above I_c. It could be considered that an increase in phytoplankton losses caused by grazing or settling would result in higher I_c values in shallow stations, and more light would be necessary to compensate the losses. This might explain the uprising of the DFM that follows the shallower Z_c resulting from the higher I_c, but, biomass losses would not account for the coupling found between the DFM locations in relation to those specific isopycnals.

Therefore, and even though the contribution of the processes already considered cannot be entirely excluded, other mechanisms must be involved in maintaining this association. Among them, the mixing and formation of water masses in the Gulf of Cádiz can be suggested to play an important role.

In attempting to elucidate the mechanism(s) responsible for the invariable appearance of the DFM at a particular density interval in the Gulf of Cádiz, the profiles of several hydrobiological variables and *T–S* diagram for a station located at 36.5°N and 7°W obtained in several different cruises (Vizconde-02/02, ARSA-03/98, GOLFO-03/00, GOLFO-04/00, GOLFO-2001, Ictioalboran-07/97, GOLFO-10/00 and Sesit-11/98) were plotted and compared (Fig. 13). According to the collected data, a deep mixing occurs in the basin during winter with σ_t values around 26.66 in the mixed layer, and the presence of the water mass identified as NACW can be established. The mixing favors the maintenance of a high nutrient concentrations throughout the entire water column. As the irradiance increases, stratification proceeds and NACW becomes SAW in surface layers. Parallel to this gradual process of water-mass formation, nutrients are consumed by phytoplankton, which leads to the generation of two masses with different characteristics: an upper one with low nutrient levels and the deeper NACW with high nutrient concentrations (Fig. 13F). The thermohaline characteristics of the SAW will depend on the conditions existing in the mixed layer during winter. In particular, in this area the maximum σ_t of SAW was 26.66 (Fig. 13), and this σ_t value marks then the limit between both water masses. The special relevance of the SAW–NACW interface is evidenced when density is analyzed in relation to nutrient concentration (Fig. 14). The strong correlation found between Z_{NN} and $Z_{26.66}$ is statistically significant (Table 4), demonstrating that the distribution of isopycnals in the Gulf controls the distribution of nutrients, especially in those stations where nutrient inpot to the surface is hindered by the absence of other possible inputs such as river discharge. When σ_t value exceeds 26.66, nutrient concentrations increase sharply (Fig. 14), always being higher than the half-saturation constant for phytoplankton growth (0.5 μM; Eppley et al., 1969). Thus, in open, unperturbed ocean stations, the seasonal cycle of water mass formation during winter will determine the position of both Z_{NN} and Z_{DFM} over the following summer, as both levels will be invariably associated to the isopycnal 26.66 regardless of the depth at which it occurs.

Besides the coupling between the DFM depth and the isopycnal $\sigma_{t26.66}$, a DFM intensification was observed towards the coast in the perturbed ocean

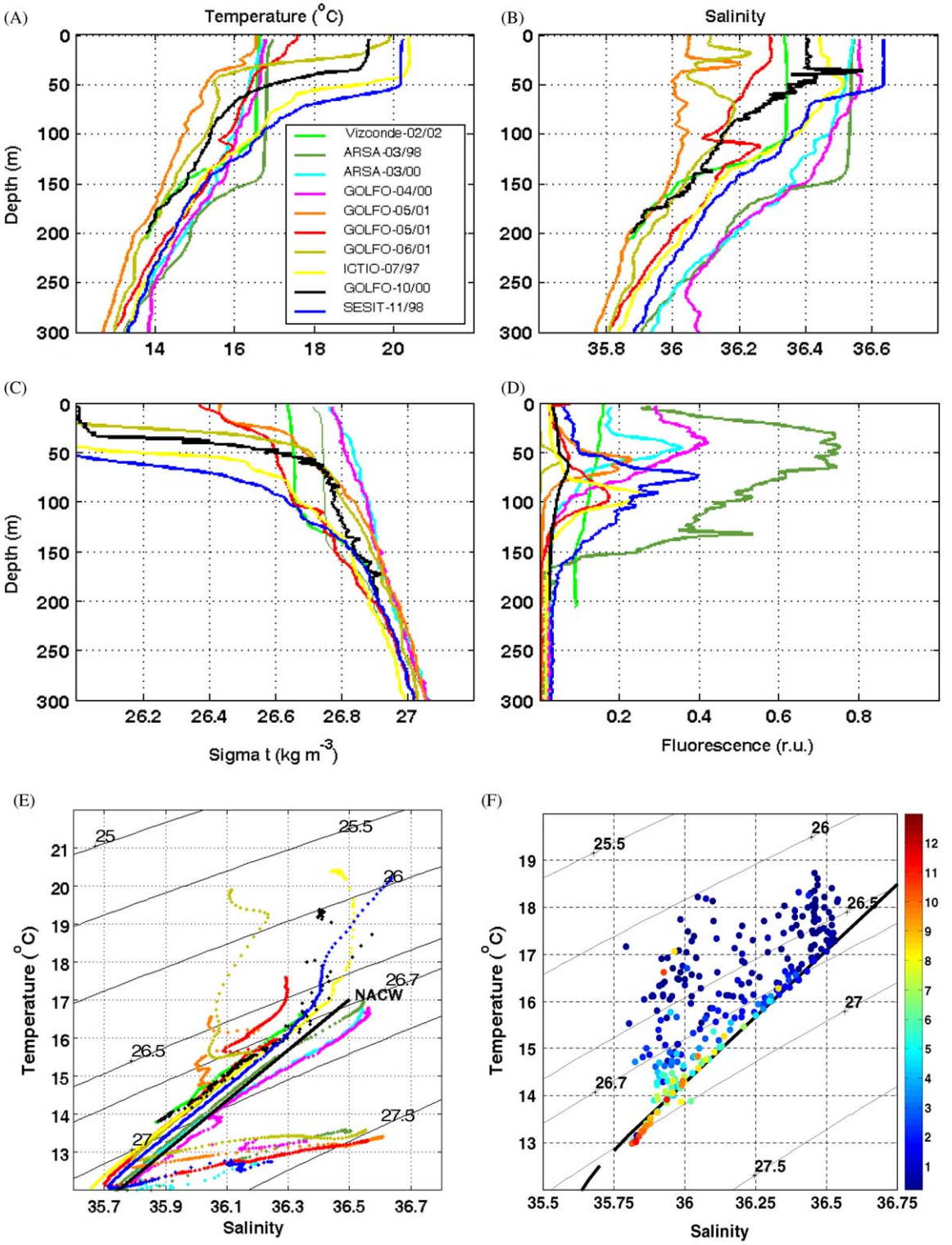

Fig. 13. Temperature (in °C, A), salinity (B), density anomaly (C) and fluorescence (in r.u., D) profiles and *T*–*S* diagrams (E) for a station located at 36.5°N–7°W obtained from data collected in different cruises carried out in the area. (F) *T*–*S* diagram and nutrient (nitrate + nitrite, μM) concentration in the Macroscale leg (GOLFO-2001). In *T*–*S* diagrams, thin lines indicate isopycnals and the thick line represents the thermohaline characteristics of NACW.

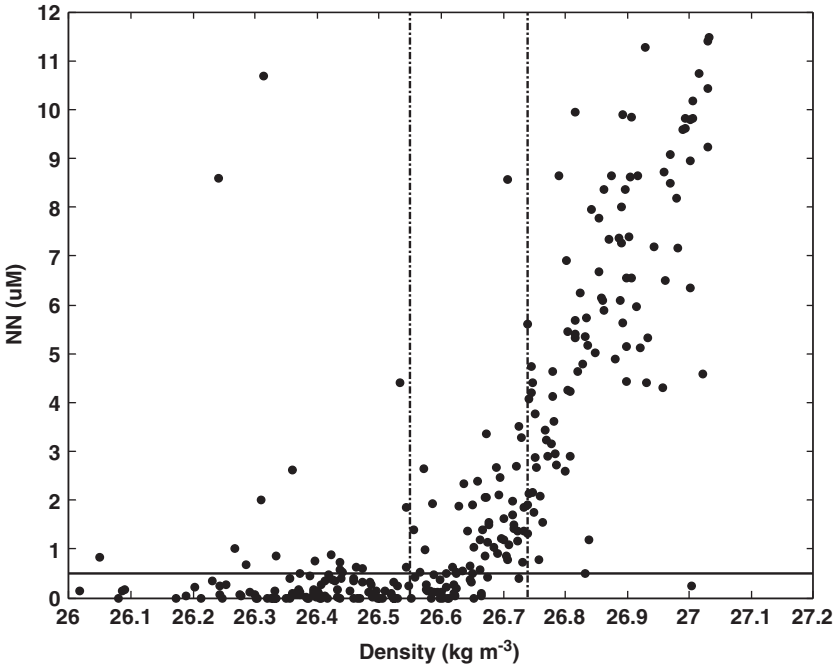

Fig. 14. Plots of nitrate plus nitrite concentrations (μM) versus density anomaly in the Macroscale leg. The solid horizontal line marks the typical value of $K_s \approx 0.5\,\mu M$, the nutrient concentration at which phytoplankton nitrate uptake is half-saturated and the vertical dashed lines show the σ_t of 26.55 and 26.74.

under the influence of coastal processes (Figs. 6 and 10). This finding could be due to two circumstances. Firstly, the incident light intensity on that isopycnal is higher than the irradiance that reaches the isopycnal in oceanic stations (Fig. 10). Therefore phytoplankton growth also is expected to be higher, which will augment the intensity of the DFM. Furthermore, radiation will not penetrate deeper through the water column, as attenuation will proceed due to phytoplankton accumulation at the DFM. Secondly, the gradient of the vertical diffusive flux, which is indicative of the phytoplankton growth associated to vertical nutrient fluxes, between the isopycnals $\sigma_{t26.55-26.74}$ where the DFM located is greater in the ocean perturbed by the influence of the coast, as was calculated following Eq. (5):

$$\text{Gradient of vertical diffusive flux} = \frac{\partial}{\partial z}\left(K_v \frac{\partial \text{Nut}}{\partial z}\right), \tag{5}$$

where K_v represents the coefficient of vertical turbulent diffusion, estimated according to the parameters of Pacanowski and Philander (1981)

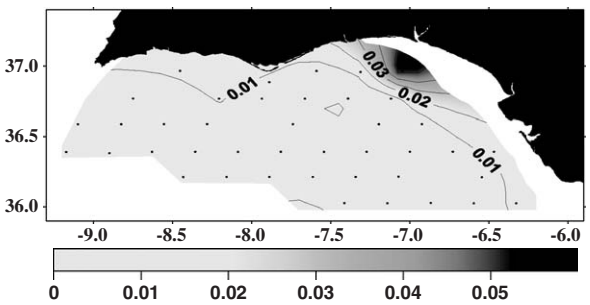

Fig. 15. Distribution of the gradient of diffusive flux for nitrate plus nitrite (mmol NN m^{-3} d^{-1}) within the σ_t interval 26.55 and 26.74 in the Macroscale leg.

and the resulting Richardson number for the Gulf obtained for this cruise (Criado-Aldeanueva et al., 2006). Fig. 15 depicts the gradient of vertical diffusive flux throughout the study area. This gradient can be then used to estimate the input of nutrients around the DFM that triggers phytoplankton proliferation and shows that the DFM intensified as approaching to coast and perturbed stations.

The horizontal diffusion flux also was calculated using the horizontal analogous of Eq. (5) with a K_H value of $3\,m^2\,s^{-1}$ (Ledwell et al., 1993). On both isopycnals considered, the computed values (not shown) for the horizontal diffusion flux were 2 orders of magnitude smaller than those corresponding to the vertical diffusive flux values; therefore, the former was considered irrelevant in this analysis.

Consequently, the seasonal cycle of water-mass formation in the Gulf determines the position of the DFM in the water column during summer in the entire area. Perturbations influence the DFM magnitude, but its position remains associated to the isopycnal 26.66.

This hypothesis on the location of the DFM allows us to predict its position in the Gulf through the information provided by a winter vertical profile of the thermohaline characteristics. This conceptual model might be extrapolated and applied to other areas in the Subtropical Northeastern Atlantic. For instance, in the Canary region during the mixing season, the upper mixing layer (around 150 m thick) exhibits values of σ_t around 26.4 (data taken from 3rd deployment in ESTOC station of the ANIMATE Project, http://www.soc.soton.ac.uk/animate). Basterretxea et al. (2002) and Tett et al. (2002) reported the DFM to be located at that particular density, and thereby the thermohaline characteristics during the preceding mixing period also determine the DFM position during the stratification period at this area. The same analysis could be extended to the Azores region (Mouriño et al., 2001).

5. Concluding remarks

The PP rates measured in the sampled region of the Gulf of Cádiz reflect the sub-tropical location of the basin, with a few sites displaying high rates due to the presence of sub-regional dynamics, such as upwelling processes or coastal mechanisms that favor phytoplankton growth. Moreover, according to the results presented here, the mechanisms responsible for the formation of surface waters masses in the Gulf throughout the seasonal cycle determine the position of the DFM in the water column rather than the classical explanation based exclusively on the attenuation of light, nutrient supply, eddy diffusion effects, etc.: which does not consider the history effects in the ecosystems. The isopycnal interval ($\sigma_{26.55-26.74}$) marks the interface between the deepest limit of the SAW and the shallowest limit of the NACW. The limit occurs at the end of the mixing season and governs when

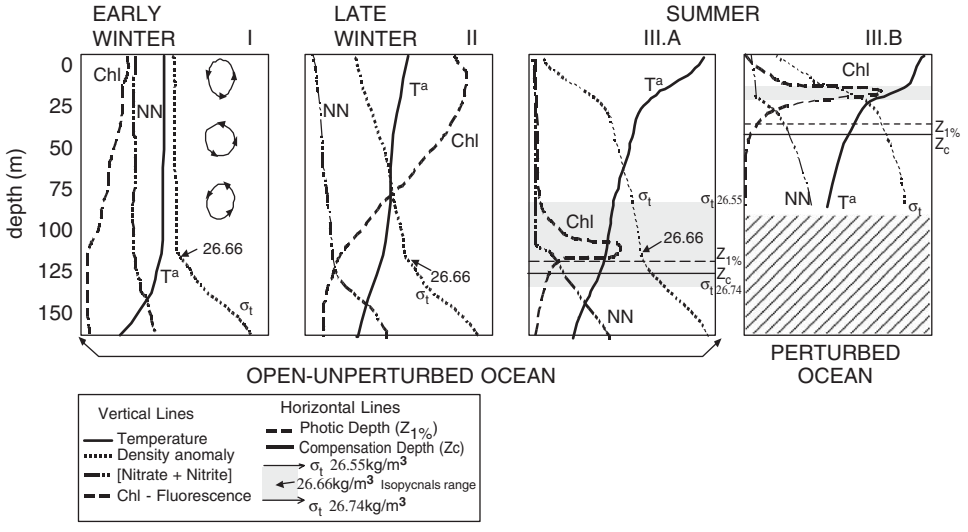

Fig. 16. Conceptual model of the mechanism explaining the DFM location in open-unperturbed and perturbed ocean stations through the mechanism of water-mass formation in the Gulf of Cádiz. The plots display several CTD profiles during the different seasons of the annual cycle: (I) winter, (II) late winter and (III) summer. During winter (the mixing season) a mixed layer occurs in the area (I) characterized by homogeneous thermohaline characteristics with σ_t values around 26.66. The mixing favors the maintenance of a high nutrient concentrations in the entire water column. During the late winter (II), while the irradiance rises, stratification proceeds in the upper layers and nutrients are consumed by phytoplankton. Over the summer period, the DFM appears invariably linked to the isopycnal of 26.66 both in open unperturbed and perturbed ocean stations. DFM would then diminish the upward flux of nutrient and the downward flux of irradiance. More details are given in the text.

nutrient concentration begins not to be limiting for phytoplankton growth. This mechanism allows one to infer the location of the DFM during the stratification period by using the density value of the mixed layer observed during the preceding winter intermediate convection. A conceptual model of this mechanism has been summarized in Fig. 16.

Acknowledgements

The authors gratefully acknowledge crew and technical staff of the R.V. *Hespérides* for their invaluable help during the cruise, Marta Sebastian and Manuel Arjonilla for their technical assistance in ^{14}C uptake experiment and nutrient analysis, respectively. The comments and suggestions of two anonymous reviewers were very helpful in clarifying our ideas for the manuscript. We also thank Dr. Laura Prieto for helpful discussions during the preparation of the manuscript. This work was supported by projects MAR99-0643-C03-02 and CTM2005-01091/MAR and G.N. by a F.P.I. fellowship from MEC.

References

Agustí, S., Duarte, C.M., 1999. Phytoplankton chlorophyll *a* distribution and water column stability in the central Atlantic Ocean. Oceanologica Acta 22 (2), 193–203.

Baldó, F., García-Isarch, E., Jiménez, M.P., Romero, Z., Sánchez-Lamadrid, A., Catalán, I.A., 2006. Spatial and temporal distribution of the early life stages of three commercial fish species in the North Eastern shelf of the Gulf of Cádiz. Deep-Sea Research II, this issue [doi:10.1016/j.dsr2.2006.04.004].

Baringer, M.O., Price, J.F., 1999. A review of the physical oceanography of the Mediterranean outflow. Marine Geology 155 (1–2), 63–82.

Basterretxea, G., Arístegui, J., 2000. Mesoscale variability in phytoplankton biomass distribution and photosynthetic parameters in the Canary–NW African coastal transition zone. Marine Ecology-Progress Series 197, 27–40.

Basterretxea, G., Barton, E.D., Tett, P., Sangrá, P., Navarro-Pérez, E., Arístegui, J., 2002. Eddy and deep chlorophyll maximum response to wind-shear in the lee of Gran Canaria. Deep-Sea Research I 49 (6), 1087–1101.

Bode, A., Varela, M., 1998. Mesoscale estimations of primary production in shelf waters: a case study in the Golfo Artabro (NW Spain). Journal of Experimental Marine Biology and Ecology 229, 111–131.

Bower, A., Armi, L., Ambar, I., 1997. Lagrangian observations of meddy formation during a Mediterranean undercurrent seeding experiment. Journal of Physical Oceanography 27, 2545–2575.

Bryden, H.L., Stommel, H.M., 1982. Origin of the Mediterranen outflow. Journal of Marine Research 40, 55–71.

Brzezinski, M.A., Villareal, T.A., Lipschultz, F., 1998. Silica production and the contribution of diatoms to new and primary production in the central North Pacific. Marine Ecology-Progress Series 167, 89–104.

Catalán, I.A., Jiménez, M.T., Alconchel, J.I., Prieto, L., Muñoz, J.L., 2006. Spatial and temporal changes of coastal demersal assemblages in the Gulf of Cadiz (SW Spain) in relation to environmental conditions. Deep-Sea Research II, this issue [doi:10.1016/j.dsr2.2006.04.005].

Cotté-Krief, M.H., Guieu, C., Thomas, A.J., Martin, J.M., 2000. Sources of Cd, Cu, Ni and Zn in Portuguese coastal waters. Marine Chemistry 71 (3–4), 199–214.

Criado-Aldeanueva, F., García-Lafuente, J., Vargas, J.M., Del Río, J., Vázquez, A., Reul, A., Sánchez, A., 2006. Distribution and circulation of water masses in the Gulf of Cádiz from in situ observations. Deep-Sea Research II, this issue [doi:10.1016/j.dsr2.2006.04.012].

Cullen, J.J., 1982. The deep chlorophyll maxumin: comparing vertical profiles of chlorophyll *a*. Canadian Journal of Fisheries and Aquatic Sciences 39, 791–803.

Davies, A.G., Sleep, J.A., 1981. The photosynthetic response of nutrient-depleted dilute cultures of *Skeletonema costatum* to pulses of ammonium and nitrate; the importance of phosphate. Journal of Plankton Research 11, 141–164.

Eppley, R.W., Rogers, J.N., McCarthy, J.J., 1969. Half-saturation constants for uptake of nitrate and ammonium by marine phytoplankton. Limnology and Oceanography 14, 912–920.

Fasham, M.J.R., Platt, T., Irwin, B., Jones, K., 1985. Factors affecting the spatial pattern of the deep chlorophyll maximum in the region of Azores front. Progress in Oceanography 14, 129–165.

Fiúza, A.F.D., de Macedo, M.E., Guerreiro, M.R., 1982. Climatological space and time variation o the Portuguese coastal upwelling. Oceanologica Acta 5 (1), 31–40.

Folkard, A.M., Davies, P., Fiúza, A.F.G., Ambar, I., 1997. Remotely sensed sea surface thermal patterrns in the Gulf of Cádiz and the Strait of Gibraltar: Variability, correlations and relationships with the surface wind field. Journal of Geophysical Research 102 (C3), 5669–5683.

Furuya, K., 1990. Subsurface chlorophyll maximum in the tropical and subtropical western Pacific Ocean: vertical profiles of phytoplankton biomass and its relationship with chlorophyll *a* and particulate organic. Marine Biology 107, 529–539.

García, C.M., Prieto, L., Vargas, M., Echevarría, F., García-Lafuente, J., Ruiz, J., Rubin, J.P., 2002. Hydrodynamics and the spatial distribution of plankton and TEP in the Gulf of Cádiz (SW Iberian Peninsula). Journal of Plankton Research 24 (8), 817–833.

García-Lafuente, J., Delgado, J., Criado-Aldeanueva, F., Bruno, M., Río, J., Vargas, J.M., 2006. Water masses circulation in the continental shelf of the Gula of Cádiz. Deep-Sea Research II, this issue [doi:10.1016/j.dsr2.2006.04.011].

Heezen, B.C., Johnson, G.L., 1969. Mediterranean undercurrent and microphysiography west of Gibraltar. Bulletin of the Institute of Oceanography 67, 1382.

Herbland, A., Le Boutellier, A., 1981. The size distribution of phytoplankton and particulate organic matter in the Equatorial Atlantic Ocean: importance of ultraseston and consequences. Journal of Plankton Research 3 (4), 659–673.

Holm-Hanssen, O., Lorenzen, C.J., Homes, R.W., Strickland, J.D.H., 1965. Fluorometric determination of chlorophyll.

Journal du Conseil. Conseil Permanent International pour l'Exploration de la Mer. 187, 9–18.

Huertas, I.E., Navarro, G., Rodríguez-Gálvez, S., Prieto, L., 2005. The influence of phytoplankton biomass on the spatial distribution of carbon dioxide in surface seawater of a coastal area of the Gulf of Cádiz (SW Spain). Canadian Journal of Botany 83, 929–940.

Huertas, I.E., Navarro, G., Rodríguez-Gálvez, S., Lubián, L.M., 2006. Temporal patterns of carbon dioxide in relation to hydrological conditions and primary production in the northeastern shelf of the Gulf of Cádiz (SW Spain). Deep-Sea Research II, this issue [doi:10.1016/j.dsr2.2006.03.010].

Johnson, J., Stevens, I., 2000. A fine resolution model of the eastern North Atlantic between the Azores, the Canary Islands and the Gibraltar Strait. Deep-Sea Research I 47, 875–899.

Joint, I., Groom, S., Wollast, R., Chou, L., Tilstone, G.H., Figueiras, F.G., Loijens, M., Smyth, T., 2002. The response of phytoplankton production to periodic upwelling and relaxation events at the Iberian shelf break: estimates by the C-14 method and by satellite remote sensing. Journal of Marine Systems 32 (1–3), 219–238.

Kirk, J.T.O., 1994. Light & Photosynthesis in Aquatic Ecosystems. Cambridge University Press, Cambridge, 509pp.

Lacombe, H., Madelain, F., Gascard, J.C., 1968. Repport sur la campagne Gibraltar I du N.O. Jean Charrot 1967. Cahiers Oceanographiques XX Année Na2.

Ledwell, J.R., Watson, A.J., Law, C.S., 1993. Evidence for slow mixing across the pycnocline from an open-ocean tracer-release experiment. Nature 364, 701–703.

Mann, K.H., Lazier, J.R.N., 1996. Dynamics of Marine Ecosystems: Biological–Physical Interactions in the Oceans, second ed. Blackwell Science, Cambridge, 394pp.

Marañón, E., Holligan, P.M., Varela, M., Mouriño, B., Bale, A.J., 2000. Basin-scale variability of phytoplankton biomass, production and growth in the Atlantic Ocean. Deep-Sea Research I 47 (5), 825–857.

McAllister, C.D., Shan, N., Strickland, J.D.H., 1964. Marine phytoplankton photosynthetis as a function of light intensity: a comparison of methods. Journal of the Fisheries Research Board of Canada 21, 159–181.

Molina, R., 1975. Contribución al estudio hidrológico y dinámica del mar de Cádiz. Revista de Geofísica XXXIV (1–2), 97–115.

Morán, X.A.G., Estrada, M., 2001. Short-term variability of photosynthetic parameters and particulate and dissolved primary production in the Alboran Sea (SW Mediterranean). Marine Ecology-Progress Series 212, 53–67.

Morán, X.A.G., Gasol, J.M., Arin, L., Estrada, M., 1999. A comparison between glass fiber and membrane filters for the estimation of phytoplankton POC and DOC production. Marine Ecology-Progress Series 187, 31–41.

Morán, X.A.G., Taupier-Letage, I., Vázquez-Dominguez, E., Ruiz, S., Arin, L., Raimbault, P., Estrada, M., 2001. Physical–biological coupling in the Algerian Basin (SW Mediterranean): influence of mesoscale instabilities on the biomass and production of phytoplankton and bacterioplankton. Deep-Sea Research I 48, 405–437.

Mouriño, B., Fernández, E., Serret, P., Harbour, D., Sinha, B., Pingree, R., 2001. Variability and seasonality of physical and biological fields at the Great Meteor Tablemount (subtropical NE Atlantic). Oceanologica Acta 24 (2), 167–185.

Navarro, G., Ruiz, J., 2006. Spatial and temporal variability of phytoplankton in the Gulf of Cádiz through remote sensing images. Deep-Sea Research II, this issue [doi:10.1016/j.dsr2.2006.04.014].

Ochoa, J., Bray, N.A., 1991. Water mass exchange in the Gulf of Cádiz. Deep-Sea Research I 38 (1), 465–503.

Paasche, E., 1973. Silicon and the ecology of marine diatoms II. Silicate-uptake kinetics in five diatoms species. Marine Biology 19, 262–269.

Pacanowski, R.C., Philander, G.H., 1981. Parameterization of vertical mixing in numerical models of tropical oceans. Journal of Physical Oceanography 11, 1443–1451.

Peliz, A., Santos, A.M.P., Oliveira, P.B., Dubert, J., 2004. Cross-shelf transport induced by eddy interaction at the southwest of Iberian Peninsula in February 2001. 4a Asambleia Luso-Espanhola de Geodesia e Geofísica, Figueira da Foz, 2004.

Platt, T., Gallegos, C.L., Harrison, W.G., 1980. Photoinhibition of photosynthesis in natural assemblages of marine phytoplankton. Journal of Marine Research 38, 687–701.

Platt, T., Sathyendranath, S., Ravindran, P., 1990. Primary production by phytoplankton: analytic solutions for daily rates per unit area of water surface. Proceedings of the Royal Society of London Series B 241, 101–111.

Prieto, L., García, C.M., Corzo, A., Ruiz, J., Echevarría, F., 1999. Phytoplankton, bacterioplankton and nitrate reductase activity distribution in relation to physical structure in the northern Alborán Sea and Gulf of Cádiz (southern Iberian Península). Boletín del Instituto Español de Oceanografía 15, 401–411.

Relvas, P., Barton, E.D., 2002. Mesoscale patterns in the Cape Sao Vicente (Iberian Peninsula) upwelling region. Journal of Geophysical Research 107 (C10), 3164.

Riley, G.A., Stommel, H., Bumpus, D.F., 1949. Quantitative ecology of the plankton of the western North Atlantic. Bulletin of the Bingham Oceanographic Collection 12, 1–169.

Rubín, J.P., Cano, N., Arrate, P., García-Lafuente, J., Escánez, J., Vargas, M., Hernández, F., 1997. El Ictioplancton, el holoplancton y el medio marino en el Golfo de Cádiz, Estrecho de Gibraltar y sector noroeste del Mar de Alborán, en julio de 1994. Informe Técnico del Instituto Español de Oceanografía 167, 44pp.

Rubín, J.P., Cano, N., Prieto, L., García, C.M., Ruiz, J., Echevarría, F., Corzo, A., Gálvez, J.A., Lozano, F., Alonso-Santos, J.C., Escánez, Juárez, A., Zabala, L., Hernández, F., García-Lafuente, J., Vargas, M., 1999. La estructura del ecosistema pelágico en relación con las condiciones oceanográficas y topográficas en el golfo de Cádiz, estrecho de Gibraltar y mar de Alborán (sector Noroeste), en julio de 1995. Inf. Téc. Inst. Esp. Oceanogr., 175, 73pp.

Ruiz, J., García-Isarch, E., Huertas, I.E., Prieto, L., Juárez, A., Muñoz, J.L., Sánchez-Lamadrid, A., Rodríguezí-Gálvez, S., Naranjo, J.M., Baldó, F., 2006. Meteorological and oceanographic factors influencing *Engraulius encrasicolus* early life stages and catches in the Gulf of Cádiz. Deep-Sea Research II, this issue [doi:10.1016/j.dsr2.2006.04.007].

Serra, N., Ambar, I., 2002. Eddy generation in the Mediterranean undercurrent. Deep-Sea Research II 49 (19), 4225–4243.

Serra, N., Sadoux, S., Ambar, I., Renouard, D., 2002. Observations and laboratory modeling of meddy generation at Cape St. Vincent. Journal of Physical Oceanography 32, 3–25.

Stevenson, R.E., 1977. Huelva Front and Malaga, Spain, Eddy Chain as defined by Satellite and Oceanographic Data. Deutsche Hydrographische Zeitschrift 30 (2), 51–53.

Tett, P., Arístegui, J., Barton, E.D., Basterretxea, G., De Armas, J.D., Escánez, J.E., Hernández-León, S., Lorenzo, L.M., Montero, N., 2002. Steady-state DCM dynamics in Canaries waters. Deep-Sea Research II 49 (17), 3543–3559.

UNESCO, 1994. Protocols for Joint Global Ocean Carbon Flux Study (JGOFS) core measurements, Manuals and Guides. 29, 170pp.

Vargas-Yañez, M., Sarhan, T., Plaza, F., Rubin, J.P., García-Martínez, M.C., 2002. The influence of tide–topography interaction on low-frequency heat and nutrient fluxes. Application to Cape Trafalgar. Continental Shelf Research 22, 115–139.

Walsh, J.J., 1988. On the nature of continental shelves. Academic Press, New York (p. 126).

Webb, W.L., Newton, M., Starr, D., 1974. Carbon dioxide exchange of *Alnus rubra*: a mathematical model. Ecologia 17, 281–291.

Wooster, W.S., Bakun, A., McLain, D.R., 1976. The seasonal upwelling cycle along the eastern boundary of the North Atlantic. Journal of Marine Research 34, 131–146.

Zenk, W., 1975. On the Mediterranean outflow west of Gibraltar. "Meteor" Forsch-Erfebn 7 (16), 23–43.

Zenk, W., Army, L., 1990. The complex spreading pattern of Mediterranean Water off Portuguese continental slope. Deep-Sea Research I 10, 221–231.